Variational Level Set Method for Topology Optimization of Origami Fold Patterns

Qian Ye1

Xianfeng David Gu²³

¹Department of Mechanical Engineering, State University of New York ³De Stony Brook, NY 11794 Email: gian.ye@stonybrook.edu

ng, ²Department of Computer Science
³Department of Applied Math and Statistics
State University of New York,
Stony Brook, NY 11794
Email: gu@cs.stonybrook.edu

Shikui Chen¹ *

¹Department of Mechanical Engineering State University of New York, Stony Brook, NY 11794 Email: shikui.chen@stonybrook.edu

ABSTRACT

With specific fold patterns, a 2D flat origami can be converted into a complex 3D structure under an external driving force. Origami inspires the engineering design of many self-assembled and re-configurable devices. This work aims to apply the level-set-based topology optimization to the generative design of origami structures. The origami mechanism is simulated using thin shell models where the deformation on the surface and the deformation in the normal direction can be simplified and well captured. Moreover, the fold pattern is implicitly represented by the boundaries of the level set function. The folding topology is optimized by minimizing a new multi-objective function designed to balance kinematic performance with structural stiffness and geometric requirements. Besides regular straight folds, our proposed model can mimic crease patterns with curved folds. With the folding curves implicitly represented, the curvature flow is utilized to control the complexity of the folds generated. The performance of the proposed method is demonstrated by the computer generation and physical validation of a thin-shell origami gripper.

1 Introduction

1.1 Origami-Inspired Design: State of the Art

Demonstrating the ability to transform from 2D to 3D, origami-inspired deployable structures have been applied in the engineering [1], such as packaging, deployable solar panels, self-deployable mechanisms, and metamaterial design [2,3,4,5]. Mathematicians examined origami from a geometric perspective to comprehend the relationship between the fold pattern and the folded status [6]. Hull [7,8] studied the relation between the folding angles and the crease patterns and delivered a theorem for the local flat-foldability. However, the theorem is insufficient for global foldability. Robert Lang applied the circle packing technique and proposed the software-TreeMaker that can compute the crease patterns from stick figures [9].

As for the analysis of the distortion of origami structures, various models have been developed. One well-adopted approach is the so-called rigid-origami, which assumes that all the deformation occurs in the folding lines, and the facets between folding lines are rigid [8,10,11]. Tachi [12,10] developed a simulation software for rigid origami. The configuration of the model, in other words, the deformed shape, is explicitly represented by crease angles, and the trajectory is calculated by projecting angle motion into the constrained space. This pioneering work provided some freedom to the user to revise the folding lines and avoid local self-intersections. However, the global self-intersection still exists. Similarly, Wei *et al.* [13] studied the periodic pleated origami using geometric mechanics. To address the problem on non-negligible fold thickness or

^{*}Address all correspondence to this author.

with maximum curvature at the folds [14], Lagoudas *et al.* [15,16] presented smooth folds model for rigid origami simulation which can simulate the realistic folds of nonzero surface area and contain higher-order geometric continuity.

However, the rigid origami model cannot completely express the actual behavior of an origami. In reality, the facet area undergoes non-negligible deformation, such as bending, stretching, and shearing. To solve the problem, Schenk and Guest [11] proposed a pin-joint framework to track the motion of a partially folded sheet with a low computational cost. Their model also links the pure kinematics to the stiffness matrix approach. Liu and Paulino [17,18] proposed a nonlinear formulation to simulate large-displacement origami structures. They simplified the bar-and-hinge model [19] as pin-jointed bar networks with virtual rotational springs for origami simulations, and thus reduced the degree of freedom and improved the computational efficiency. The model can globally capture the essential features of origami, including folding, bending, and multi-stability. Based on the bar-and-hinge model, Ghassaei *et al.* [20] introduced a high-speed origami simulator using a Graphics Processing Unit (GPU). This work is promising regarding the computational speed and interactivity that offering real-time simulation and interaction. However, compromises have to be considered between geometric accuracy and simulation speed, and instability will occur on facets with high-aspect-ratio triangles. Another engineering approach is by using shell or membrane element in finite element analysis to simulate the deployment of the origami [21,22]. Cai *et al.* [22] conducted the nonlinear finite element analysis using the variable Poisson's ratio model to revise the stress distribution of membrane element and successfully tracked the deployment of the famous Miura-ori pattern.

Recently, in the field of computer graphics and architectures, the studies of origami with curved folds are emerging [23, 24, 25], since its potential in kinetic systems for architectural application [26] and shape-programmable structures [27, 28]. In the design of the complaint mechanism, Nelson *et al.* [29] addressed the importance of curved origami in designing developable structures. Their subsequent work [30, 31, 32] presented an energy method based on the normalized coordinate equations to identify the natural configurations of general curve folds. Moreover, in engineering, one of the significant applications of flexible electronics- the wearable soft electronics, complaint origami with curved creases- is more desirable because of easier conformal to the human body than conventional rigid origami.

Conventionally, the design of origami is based on the analysis and alteration of several well-known crease patterns. Fuchi *et al.* [33,34] did some pioneering work on topology optimization of origami structures. They proposed an optimization framework to achieve an optimal origami design by adding or removing folding lines to or from a reference crease pattern. Later, they enriched the work with a nonlinear truss model to model the sequenced motion and the large deformation of an origami [35,36]. In addition, a recent work proposed by Paulino *et al.* [37] offered a novel perspective of generating origami design. They applied a shape grammar formalism and coupled with an interpreter to construct and modify an origami tessellation. These origami design frameworks are mainly based on rigid-origami, which are composed of rigid patches with straight creases working as rotational joints.

1.2 Topology Optimization

Topological optimization aims to find the best design geometry for optimal performance under certain constraints. The density-based approach, such as the homogenization method [38, 39, 40] and the Solid Isotropic Material with Penalization (SIMP) method [41, 42], is the most popular way of doing topology optimization on the surface. However, the design obtained by the density-based optimization method can contain checkerboard patterns or grey elements. In contrast to the density-based method, the level set method can provide a clear boundary design. Moreover, since the level set functions are defined in the space with one higher dimension, the higher-order geometric information, such as curvatures and normal vectors, is embedded naturally in the geometric model. It allows the level set method for an exclusive capability of dealing with topological changes [43]. The level-set-based topology optimization (TO) approach has been considered a powerful tool in generating innovative designs ever since the shape sensitivity analysis was cast into the framework [44, 45, 46, 47].

In this work, a systematic solution to simulate and conceive origami-inspired compliant structures is presented. We integrate the shell model with the level-set topology optimization framework. The origami is modeled utilizing finite element analysis with shell elements. Thus the in-plane membrane, out of plane bending and shear deformation, can be well captured. Moreover, by incorporating the level-set based topology optimization method, the crease patterns are represented implicitly by the boundaries of the level set functions. The optimization problem is formulated as a multi-objective problem that aims to achieve an optimal distribution of the folding lines to fulfill the prescribed requirements. The topology of the crease pattern is optimized by solving the PDE, the so-called Hamilton-Jacobi equation. Rather than adopting straight folding lines, our optimization method can form curved folds.

The remainder of the paper is organized as follows: Section. 2 introduces the background on level-set-based topology optimization framework and the shell model for simulating origami structures. In Section. 3, we formulate the problem of optimizing origami structures and provide the sensitivity analysis. Next, an example of an origami gripper and an origami twisting mechanism are presented in Section. 4. Section. 5 first discusses the effects of initial designs and then shows the performance of the objective function through a numerical example. Finally, in Section. 6, the conclusions are drawn, and the future work is also briefly discussed.

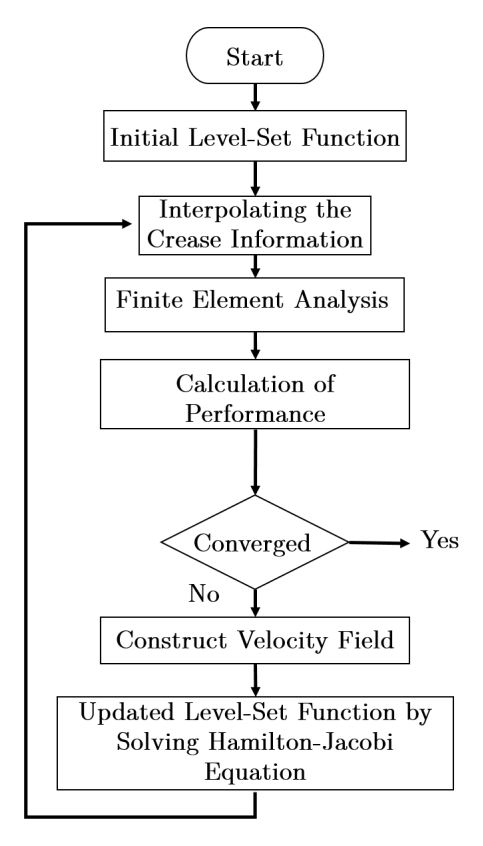


Fig. 1: The flow chart

2 Method Overview

In this work, we propose a solution to systematic modeling and optimization of the origami structures to meet the mechanical requirements. The method is based on the level-set topology optimization framework and a modified shell model. The flow chart is shown in Fig. 1.

2.1 Level Set Representation for Origami Structures

In this work, a level set representation for topology optimization of an origami structure is proposed. Basically, we divide the design domain into two sections: the crease (folding line) and the facet area. A convex (concave) crease is called the mountain, or valley, fold line. Thus, two level set functions are introduced. Similar as the conventional level set method, the level set functions ϕ are defined in \mathbb{R}^2 or \mathbb{R}^3 as a implicit function on one higher dimension [44]. The boundaries of each level set functions represent the mountain and valley folds, respectively, and the areas apart from boundary are the facets as shown in Eq. 1.

$$\begin{cases} \phi^{k}(\mathbf{x},t) = 0, & x \in \Gamma^{k}(t), k = V, M, \text{folding lines} \\ \phi^{k}(\mathbf{x},t) \neq 0, & x \in D \backslash \Gamma^{k}(t), \text{facet} \end{cases}$$
 (1)

where D is a bounded area represents the design domain and $D \subset \mathbb{R}$. \mathbf{x} is a point inside the design domain. k represents the different level set functions. In our case, the number of k is 2. M and V represent the mountain folds and valley folds, respectively as shown in Fig. 2.

The crease pattern's topology is optimized by solving the Hamilton-Jacobi equation as Eq. 2, which is defined by differentiating the level set function with respect to the time t [44].

$$\frac{\partial \phi^k}{\partial t} - \mathbf{V}^k \cdot \nabla \phi^k = 0, \tag{2}$$

where $V^k = \dot{x}$ is the velocity field for the folding line. During the topology optimization, each level set function involves individually. Thus, in the rest of the paper, for simplicity, we use ϕ to represent a general level set function unless otherwise

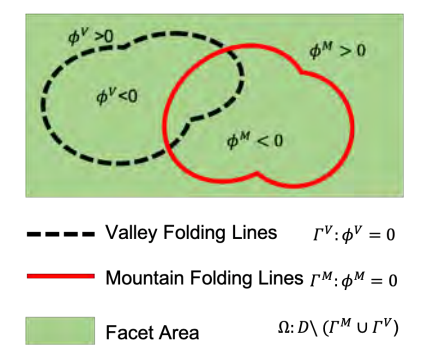


Fig. 2: A schematic of the level set representation of an origami structure

stated. The presented Hamilton- Jacobi equation can be solved using the upwind spatial derivative to update the design iteratively [45]. A velocity extension step is needed to expand the normal velocity from the boundaries to the whole computational domain. In our case, the natural extension method is applied since the strain field is defined on the entire design domain [48].

Instead of assuming straight folding lines, with our model, we can form a general fold pattern with both regular straight folds as long as curved ones. With the level set method, higher-order geometric information, such as curvature, can be used to control the length and straightness of the generated crease patterns.

2.2 The Shell Model for Simulating Origami Structures

The origami mechanism is simulated using shell models where the in-plane membrane, out of plane bending, and shear deformation can be well captured. For simplicity, at this point, we assume the problem to be linear elastic. The crease is considered a region of locally weak material with directional imperfections on the shell. A similar technique has been used in studying shells with curved creases [28], and the collapse of a thin-walled tubular [49]. We define the thickness and Young's modules on the crease to be half of those in the facet area.

$$t_{facets} = 2t_{folds},$$

$$E_{facets} = 2E_{folds},$$
(3)

where *t* is the local thickness, and *E* represents Young's modules. Moreover, we modify the local offset plane in the area near the crease with a sign relevant to the crease type as shown in Fig. 3. The fold locations are determined by the boundary of the level set functions calculated by the following smoothed delta function [45].

$$\delta(\phi) = \begin{cases} \frac{1}{2\varepsilon} + \frac{1}{2\varepsilon} cos(\frac{\pi\phi}{\varepsilon}) & -\varepsilon \le \phi \le \varepsilon \\ 0 & else \end{cases}$$
 (4)

where ε controls the size of the transition area, which is chosen as two times the mesh size [47,43]. Then we normalize the $\delta(\phi)$ to $\hat{\delta}(\phi)$, where the maximum value is equal to 1, and couple the $\hat{\delta}(\phi)$ on the shell model. The scheme of the level set representation of a modified shell model is shown in Fig. 3. It is worth noting that the smoothed delta function can provide a gradual transaction in the thickness direction. The middle surface location \mathbf{r} of the shell model can be represented as [50,51].

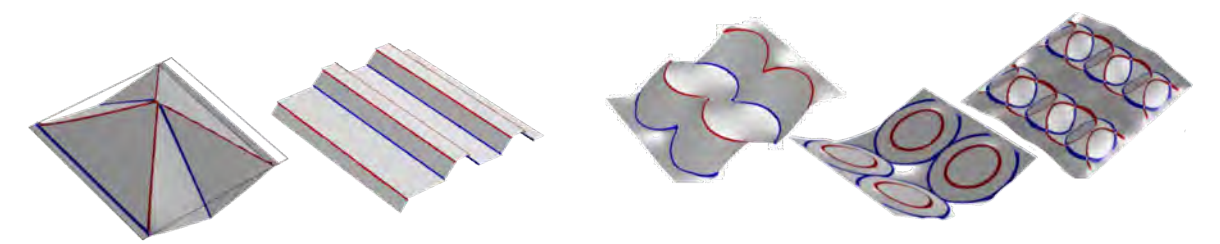
$$\mathbf{r}\left(\xi^{1},\xi^{2}\right) = \mathbf{r}_{R}\left(\xi^{1},\xi^{2}\right) + \zeta_{0}\mathbf{n}\left(\xi^{1},\xi^{2}\right) \tag{5}$$

where \mathbf{r}_R is the meshed surface, ξ_1, ξ_2 are the two curvilinear coordinates in the middle surface, and \mathbf{n} is the normal direction on the shell. The ζ_0 is the offset in the thickness direction, which related to $\hat{\delta}(\phi)$ as Eq. 6.

$$\zeta_0 = \begin{cases}
+\hat{\delta}(\phi)_M \times \frac{1}{2} \times t_{\text{folds}}, & \text{on mountain folds} \\
0, & \text{on facet area} \\
-\hat{\delta}(\phi)_V \times \frac{1}{2} \times t_{\text{folds}}, & \text{on valley folds}
\end{cases}$$
(6)



Fig. 3: The schematic of level set representation of a modified shell model



(a) Modelling of origami structures with straight folds

(b) Modelling of origami structures with curved folds

Fig. 4: Origami structures modeled by modified shell

The strain of the undeformed middle surface can be evaluated as the following equation.

$$\frac{\partial \mathbf{r}}{\partial \xi^{\alpha}} = \frac{\partial \mathbf{r}_{R}}{\partial \xi^{\alpha}} + \zeta_{0} \frac{\partial \mathbf{n}}{\partial \xi^{\alpha}} \tag{7}$$

where α ranges from 1 to 2. Thus, with the offset, an extra term is added onto the strain, and acts as a small perturbation to model. We testify the modified shell model with different crease patterns with both straight and curved folds, and their deformed shapes are shown in Fig. 4. It is worth noting that the physics properties of the intersections between mountain and valley folding lines have already been implied. The thickness and Youngs modulus still follow the creases ones, but the offsets in the thickness direction cancel out. Thus, the overlaps are essentially areas with weak material but without the in-thickness offsets.

In the finite element analysis of the continuum shell, we adopt the classic Mindlin-Reissner plate shell theory that takes into account the through-thickness shear deformation [52, 53, 54]. The background information regarding the shell model and the derivation of the linear elastic strain energy density is introduced in the Appendix.A. In terms of the numerical implementation, the SC6R element is applied, which consists of 6 nodes, and each node has six degrees of freedom (DOF) in 3D in which including three translational DOF and three rotational DOF [53, 54, 55].

3 Problem Formulation and Shape Sensitivity Analysis

The topology optimization of an origami mechanism is equivalent to finding the optimum crease pattern to meet the engineering design requirements. In this work, we solve the optimization problem by minimizing a multi-objective function, which comprises three sections:

- the the engineering target (J_1) to meet the kinematic requirements;
- the characteristic requirements for the design to be an origami structure (J_2) ;
- the perimeter constraint for achieving concise designs.

The general objective function can be formulated as follows:

Minimize:
$$J = I_1 J_1 + I_2 J_2 + \alpha |\partial \Omega|$$
,
Subject to: $a(\mathbf{u}, \mathbf{v}) = l(\mathbf{v}), \forall \mathbf{v} \in U_{ad}$. (8)

In the equation above, U_{ad} is the space kinematically admissible displacement [56], Ω is the region occupied with the linear elastic material. I_1 , I_2 , and α are constant weighting factors for kinematic target, characteristic objective and perimeter

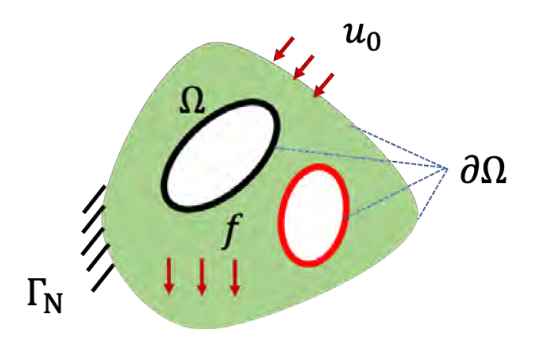


Fig. 5: A schematic of general boundary condition

constraint. The internal virtual energy a(u,v), and exterior virtual energy l(v) are defined as follows:

$$a(\boldsymbol{u}, \boldsymbol{v}) = \int_{\Omega} \varepsilon_{ij}(\boldsymbol{u}) \mathbb{C}_{ijkl} \varepsilon_{kl}(\boldsymbol{v}) d\Omega,$$

$$l(\boldsymbol{v}) = \int_{\Omega} f \cdot \boldsymbol{v} d\Omega + \int_{\Gamma_N} g \cdot \boldsymbol{v} d\Gamma,$$
 (9)

where D is the design domain; $\Gamma = \partial \Omega$ is the boundary of the design; a(u,v) is a symmetric bi-linear function in terms of the displacement u and the test function v, that is, a(u,v) = a(v,u); l is a linear function in terms of the body force f and the traction force g on the Neumann boundary conditions Γ_N , as illustrated in Fig. 5. We treat each of the objectives as a subproblem and can make sensitivity analysis for each subproblem and collate the results. It is known that the sensitivity analysis result of the perimeter constraint is the mean curvature κ and can be calculated by [57]:

$$\kappa = -\nabla \cdot \left(\frac{\nabla \phi}{|\nabla \phi|}\right) \tag{10}$$

Therefore, we will only show the detailed steps for sensitivity analysis of the kinematic (J_1) and the characteristic requirements (J_2) .

3.1 Shape Sensitivity Analysis of the Kinematic Objective

Here, we adapt the classic objective function of kinematic requirement—the least square minimization between the displacement u and a given target displacement u_0 of a selected zone w(x) in the design domain. w(x) is zero excepted on the selected area

Minimize:
$$J_1 = \left[\int_{\Omega} w(x) |\boldsymbol{u} - \boldsymbol{u}_0|^2 d\Omega \right]^{\frac{1}{2}},$$

Subject to: $a(\boldsymbol{u}, \boldsymbol{v} = l(\boldsymbol{v}), \forall \boldsymbol{v} \in U_{ad})$ (11)

The Lagrangian of the optimization problem is

$$L_1(\mathbf{u}, \mathbf{v}) = J_1 + a(\mathbf{u}, \mathbf{v}) - l(\mathbf{v}).$$
 (12)

The material derivative of the Lagrangian equation respect to a pseudo time t is formulated as:

$$\frac{dL_1(\boldsymbol{u},\boldsymbol{v})}{dt} = \frac{\partial L_1(\boldsymbol{u},\boldsymbol{v})}{\partial t} + \frac{\partial L_1(\boldsymbol{u},\boldsymbol{v})}{\partial \Omega},\tag{13}$$

where the partial derivative with respect to time results in the so-called adjoint equation:

$$\frac{\partial L_1(\mathbf{v})}{\partial t} = L_1' = c_0 \int_{\Omega} w(x) (\mathbf{u} - \mathbf{u}_0) \cdot u' d\Omega + a(\mathbf{u}', \mathbf{v}), \tag{14}$$

where

$$c_0 = \left[\int_{\Omega} w(x) |\mathbf{u} - \mathbf{u}_0|^2 d\Omega \right]^{-\frac{1}{2}}$$
 (15)

The convection term of the material derivative forms the shape derivative which is formulated as follows:

$$\frac{\partial L_1(\boldsymbol{u},\boldsymbol{v})}{\partial \Omega} = \int_{\Gamma} \frac{c_0}{2} w(x) |\boldsymbol{u} - \boldsymbol{u}_0|^2 \boldsymbol{V}_{n1} ds + \int_{\Gamma} \varepsilon_{ij}(\boldsymbol{u}) \mathbb{C}_{ijkl} \varepsilon_{kl}(\boldsymbol{v}) \boldsymbol{V}_{n1} ds - \int_{\Gamma} f \cdot \boldsymbol{v} \, \boldsymbol{V}_{n1} ds - \int_{\Gamma} [\frac{\partial (g \cdot \boldsymbol{v})}{\partial n} + \kappa g \cdot \boldsymbol{v}] \boldsymbol{V}_{n1} ds.$$
 (16)

Using steepest decent method while neglecting body force and traction force, the normal velocity can be written as:

$$V_{n1} = -\left[\frac{c_0}{2}w(x)|\mathbf{u} - \mathbf{u}_0|^2 + \varepsilon_{ij}(\mathbf{u})\mathbb{C}_{ijkl}\varepsilon_{kl}(\mathbf{v})\right]. \tag{17}$$

3.2 Shape Sensitivity Analysis of the Characteristic Objective

Since an origami structure shows the characteristic of the deformation concentrated on the folding lines, the facets are mainly flat, and the system undergoes large out of plane deformation [19]. Thus, we remount the objective functions by optimizing a structure which, under a load scenario, the deformation of the system is preferred to satisfy the following requirements:

- 1. The deformation occurs mainly in the crease area. J_{2_1}
- 2. The out of plane deformation dominates. $J_{2_{\rm II}}$

The $J_{2_{\text{I}}}$ and $J_{2_{\text{II}}}$ can be represented as following equations:

$$J_{2_{\text{I}}} = a(\boldsymbol{u}, \boldsymbol{u}) - a_{\Gamma}(\boldsymbol{u}, \boldsymbol{u}),$$

$$J_{2_{\text{II}}} = \frac{1}{a_{b}(\boldsymbol{u}, \boldsymbol{u})}.$$
(18)

where $a(\mathbf{u}, \mathbf{u})$ is the total strain energy, $a_{\Gamma}(\mathbf{u}, \mathbf{u})$ is the total strain energy on the creases, and $a_b(\mathbf{u}, \mathbf{u})$ is the total bending energy.

$$a_{\Gamma}(\boldsymbol{u},\boldsymbol{v}) = \int_{\tau} \varepsilon_{ij}(\boldsymbol{u}) \mathbb{C}_{ijkl} \varepsilon_{kl}(\boldsymbol{u}) ds,$$

$$a_{b}(\boldsymbol{u},\boldsymbol{u}) = \int_{\Omega} \varepsilon_{ij}^{b}(\boldsymbol{u}) \mathbb{C}_{ijkl} \varepsilon_{kl}^{b}(\boldsymbol{u}) d\Omega.,$$
(19)

We can formulate the characteristic objective function J_2 as:

$$J_2 = J_{2_{\rm I}} J_{2_{\rm II}} \tag{20}$$

Then the shape derivative of the J_2 can be represented as:

$$D_{\Omega}J_{2} = J_{2\Pi}D_{\Omega}J_{2\Pi} + J_{2\Pi}D_{\Omega}J_{2\Pi}. \tag{21}$$

where $D_{\Omega}() = \frac{\partial()}{\partial\Omega()}$. In the next sections, we formulate the objective into two subproblems and derive the sensitivity for $D_{\Omega}J_{2_{\text{I}}}$ and $D_{\Omega}J_{2_{\text{II}}}$ separately.

3.2.1 Minimizing the deformation in the facet area

We summarise the first condition as an objective function $J_{2_{\rm I}}$ which minimizes the difference of total strain energy a(u,u) and the total strain energy on the creases $a_{\Gamma}(u,u)$, as shown in Eq. 22

Minimize:
$$J_{2_{\text{I}}} = a(\boldsymbol{u}, \boldsymbol{u}) - a_{\Gamma}(\boldsymbol{u}, \boldsymbol{u}),$$

Subject to: $a(\boldsymbol{u}, \boldsymbol{v}) = l(\boldsymbol{v}), \forall \boldsymbol{v} \in U_{ad}$ (22)

The Lagrangian of the optimization problem can be formulated as follows:

$$L_2 = a(\boldsymbol{u}, \boldsymbol{v}) - a_{\Gamma}(\boldsymbol{u}, \boldsymbol{v}) + a(\boldsymbol{u}, \boldsymbol{v}) - l(\boldsymbol{v}). \tag{23}$$

The material time derivative of the Lagrangian equation can be calculated as:

$$\frac{dL_2}{dt} = \frac{\partial L_2}{\partial t} + \frac{\partial L_2}{\partial \Omega},\tag{24}$$

$$\frac{\partial L_2}{\partial t} = 2a\left(\mathbf{u}', \mathbf{u}\right) - 2a_{\Gamma}\left(\mathbf{u}', \mathbf{u}\right) + a\left(\mathbf{u}', \mathbf{v}\right) \tag{25}$$

and

$$\frac{\partial L_2}{\partial \Omega} = \int_{\tau} \varepsilon_{ij}(\boldsymbol{u}) \mathbb{C}_{ijkl} \varepsilon_{kl}(\boldsymbol{u}) \boldsymbol{V}_{n2I} ds - \int_{\tau} \left[\frac{\partial \varepsilon_{ij}(\boldsymbol{u}) \mathbb{C}_{ijkl} \varepsilon_{kl}(\boldsymbol{u})}{\partial n} + \kappa a(\boldsymbol{u}, \boldsymbol{u}) \right] \boldsymbol{V}_{n2I} ds + \int_{\tau} \varepsilon_{ij}(\boldsymbol{u}) \mathbb{C}_{ijkl} \varepsilon_{kl}(\boldsymbol{v}) \boldsymbol{V}_{n2I} ds. \tag{26}$$

The adjoint equation Eq. 25 can be expressed as:

$$\frac{\partial L_2}{\partial t} = 2 \int_{\Omega} \varepsilon_{ij}(\mathbf{u}') \mathbb{C}_{ijkl} \varepsilon_{kl}(\mathbf{u}) d\Omega - 2 \int_{\Omega} \varepsilon_{ij}(\mathbf{u}') \mathbb{C}_{ijkl} \varepsilon_{kl}(\mathbf{u}) \delta(\phi) |\nabla \phi(x)| d\Omega + \int_{\Omega} \varepsilon_{ij}(\mathbf{u}') \mathbb{C}_{ijkl} \varepsilon_{kl}(\mathbf{v}) d\Omega, \tag{27}$$

where v is the adjoint variable and is achieved by solving Eq. 27 using finite element method.

3.2.2 Maximizing the out-of-plane deformation

The second characteristic requirement $J_{2_{\text{II}}}$ can be formulated as maximization of the bending energy on the crease patterns. With the observation that in the FEM model, the bending energy is concentrated on the area near the crease, we further simplify the objective function as maximum the bending energy on the design domain. As such, the objective function can be formulated as:

Minimize:
$$J_{2_{\text{II}}} = \frac{1}{a_b(\boldsymbol{u}, \boldsymbol{u})},$$
 (28)
Subject to: $a(\boldsymbol{u}, \boldsymbol{v}) = l(\boldsymbol{v}), \forall \boldsymbol{v} \in U_{ad}$

the optimization problem becomes:

$$L_3 = \frac{1}{a_b(\boldsymbol{u}, \boldsymbol{u})} + a(\boldsymbol{u}, \boldsymbol{v}) - l(\boldsymbol{v}). \tag{29}$$

The material time derivative can be formulated as follows:

$$\frac{dL_3}{dt} = \frac{\partial L_3}{\partial t} + \frac{\partial L_3}{\partial \Omega} \tag{30}$$

where

$$\frac{\partial L_3}{\partial t} = \frac{-2a_b(\boldsymbol{u}', \boldsymbol{u})}{a_b(\boldsymbol{u}, \boldsymbol{u})^2} + a(\boldsymbol{u}', \boldsymbol{v}) - \beta \int_{\Gamma} \boldsymbol{u}' \boldsymbol{v} d\Gamma_D,
\frac{\partial L_3}{\partial \Omega} = \frac{-1}{a^2(\boldsymbol{u}, \boldsymbol{u})} \int_{\Gamma} \varepsilon_{ij}^b(\boldsymbol{u}) \mathbb{C}_{ijkl} \varepsilon_{kl}^b(\boldsymbol{u}) \boldsymbol{V}_{n2II} ds + \int_{\Gamma} \varepsilon_{ij}(\boldsymbol{u}) \mathbb{C}_{ijkl} \varepsilon_{kl}(\boldsymbol{v}) \boldsymbol{V}_{n2II} ds.$$
(31)

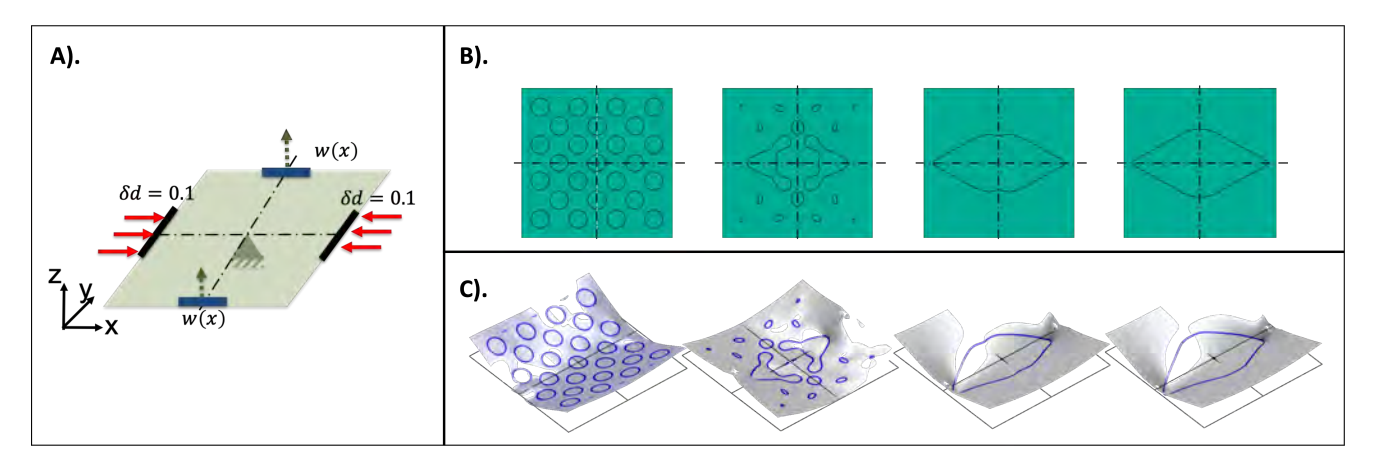


Fig. 6: Topology Optimization of an origami twister: A). boundary conditions; B). the evolution on 2D; C). the deformed status on 3D

To solve the adjoint variable v, we solve the adjoint equation

$$a(\mathbf{u}', \mathbf{v}) - \frac{2a_b(\mathbf{u}', \mathbf{u})}{a_b(\mathbf{u}, \mathbf{u})^2} - \beta \int_{\Gamma} \mathbf{u}' \mathbf{v} d\Gamma_D = 0.$$
(32)

Now we can substitute the shape gradient of each sections into Eq.21, assuming body force is zero and ignoring the velocity along the zero-length Neumann boundary, the shape gradient of the objective function is:

$$D_{\Omega}J_2 = \int_{\Gamma} GV_{n2}d\Gamma_D \tag{33}$$

Thus, by applying steepest decent method, the normal velocity can be written as:

$$V_{n2} = -G, (34)$$

where

$$G = a_{b}(\boldsymbol{u}, \boldsymbol{u}) \left[\varepsilon_{ij}(\boldsymbol{u}) \mathbb{C}_{ijkl} \varepsilon_{kl}(\boldsymbol{u}) - \frac{\partial \varepsilon_{ij}(\boldsymbol{u}) \mathbb{C}_{ijkl} \varepsilon_{kl}(\boldsymbol{u})}{\partial \boldsymbol{n}} - \kappa a(\boldsymbol{u}, \boldsymbol{u}) + \varepsilon_{ij}(\boldsymbol{u}) \mathbb{C}_{ijkl} \varepsilon_{kl}(\boldsymbol{v}) \right]$$

$$+ \left[a(\boldsymbol{u}, \boldsymbol{u}) - a_{\Gamma}(\boldsymbol{u}, \boldsymbol{u}) \right] \left[\frac{-1}{a^{2}(\boldsymbol{u}, \boldsymbol{u})} \varepsilon_{ij}^{b}(\boldsymbol{u}) \mathbb{C}_{ijkl} \varepsilon_{kl}^{b}(\boldsymbol{u}) + \varepsilon_{ij}(\boldsymbol{u}) \mathbb{C}_{ijkl} \varepsilon_{kl}(\boldsymbol{v}) \right]$$

$$(35)$$

4 Numerical Implementation

4.1 An Origami Gripper Design

In this section, we present an optimization example to test the performance of the method. The objective is to obtain an origami mechanism with a minimum crease number where the target area(s) would reach a displacement in the target direction. In other words, the optimized structure can transfer force and displacement from the input port area to the output port by deformation on the optimized origami.

Minimize:
$$J = I_1 \left[\int_{\Omega} w(x) |\boldsymbol{u} - \boldsymbol{u}_0|^2 d\Omega \right]^{\frac{1}{2}} + I_2 \frac{a(\boldsymbol{u}, \boldsymbol{u}) - a_{\Gamma}(\boldsymbol{u}, \boldsymbol{u})}{a_b(\boldsymbol{u}, \boldsymbol{u})} + \alpha |\partial\Omega|,$$

Subject to: $a(\boldsymbol{u}, \boldsymbol{v}) = l(\boldsymbol{v}), \forall \boldsymbol{v} \in U_{ad}.$ (36)

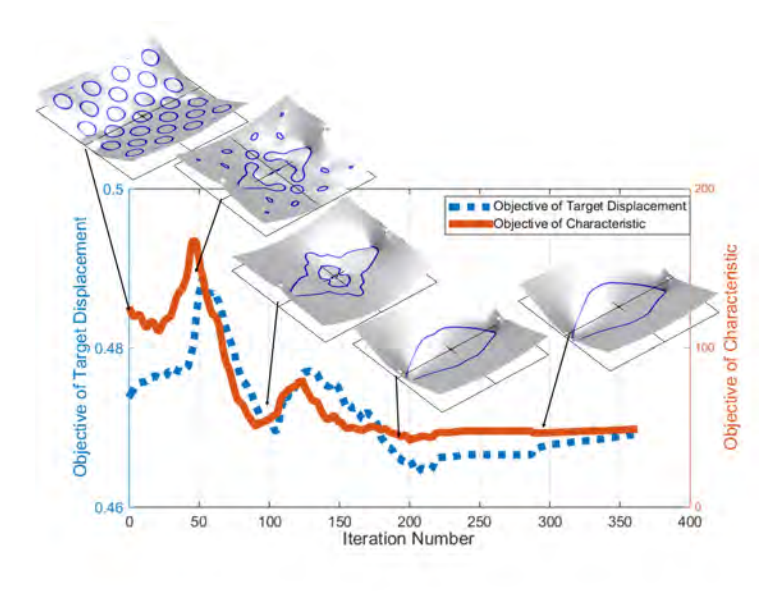
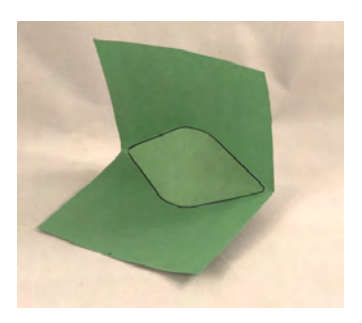


Fig. 7: The optimization history of the origami gripper



(a) The fabricated origami gripper



(b) The folded origami gripper

Fig. 8: Fabricated prototype

where I_1 , I_2 , and α are constants that weights the kinematic target, characteristic objective, and perimeter constraint. In order to reduce the difficulty of adjusting the weighting factors, a linear relationship is set as $I_2 = 1 - I_2$. Thus, the velocity filed can be represented as:

$$Vn = I_1 V_{n1} + I_2 V_{n2} + \alpha \kappa \tag{37}$$

The design domain is a 1-by-1 square, with a thickness of 0.003. The boundary conditions are shown in Fig. 6. A). In the x-direction, the input displacements are set as 0.1, as shown in Fig. 6. A). The center point is fixed. The output areas w(x) are 0.1-by-0.05 rectangles in the middle of the top and bottom sides. The target displacement u_0 is set to (0,0,1). Due to the symmetry, the upper left quarter of the domain is discretized with a rectangular 100×100 mesh. The Young's modulus is $10^6 Pa$ on the facet and $5 \times 10^5 Pa$ on the folding lines.

The evolution of the 2D design is shown in Fig. 6. B), and the corresponding deformed status is shown in Fig. 6. C). Initially, the design is a flat thin-shell consisting of circular valley folds. It can be observed that the design evolves from a group of uniformly distributed circles to a concise crease pattern. The optimization history plot is shown in Fig. 7. The plots fluctuate during the first 50 iterations, where the topology of the design changes significantly; then, after 200 iterations, the perimeter constraint dominates, so that helps smooth the folding lines and the objective curve changes to stability. Finally, both objective plots converge around the 300th iteration.

Fig. 8a is the fabricated prototype. As shown in Fig. 8b, the top and bottom of the gripper can be closed up by pushing the middle portion of both sides.

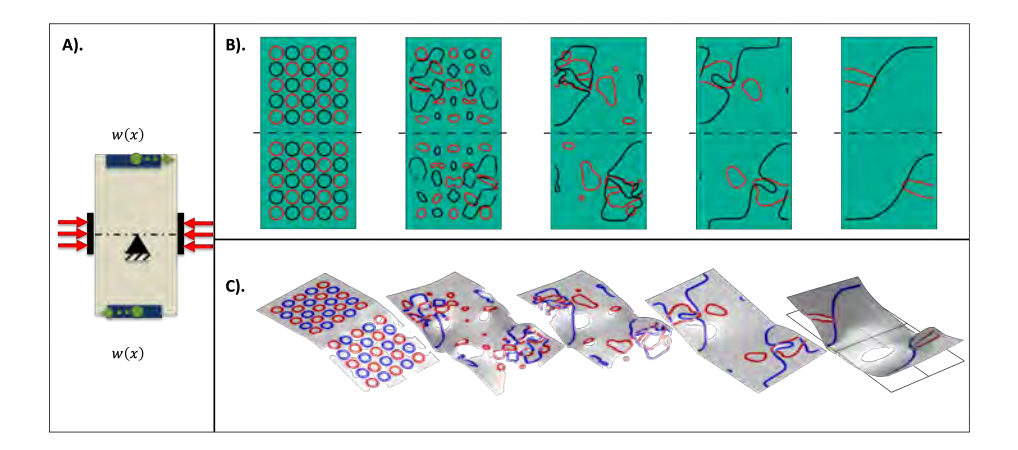


Fig. 9: Topology Optimization of an origami twister:A). boundary conditions; B). the evolution on 2D; C). the deformed status on 3D

4.2 An Origami Twister Design

This example shows a twister design. The design domain is set to be a 1 by 0.5 rectangle, and its thickness is 0.003. The objective function consists of the mechanic requirements, the characteristic part, and the mean curvature control. The target of the design is set to achieve a twist motion on the tip areas of the rectangle. The boundary condition are shown in Fig. 9.A). On the two side edges, the prescribed displacement in the x-direction is set as 0.1. The center area of the design domain is fixed. The output areas w(x) are 0.2-by-0.05 rectangles in the middle of the top and bottom sides. The target displacement on the top window is set to (0.1,0,0.1) and (-0.1,0,0.1) on the bottom. The asymmetric boundary condition is applied on the horizontal centerline of the rectangle. The upper domain is selected as the computational domain and discretized with a rectangular 100×50 mesh. The Young's modulus is $10^6 Pa$ on the facet and $5 \times 10^5 Pa$ on the folding lines.

The evolution of the 2D design, as well as their deformed status, are shown in Fig. 9. The initial design are two groups of circular folding lines which been evenly distributed in the design domain. We can observe that the final design is bending outward, which is satisfied with the target Fig. 10 plots the displacement distribution in the x-direction, and the final design is shown on the lower side of the figure.





Fig. 10: Prototype of the twister: A). The fabricated twister; B). The folded status

5 Discussion on the Initial Designs and the Characteristic Objective

5.1 The Effects of the Initial Design

To test the robustness of the method, we solve the problem again using different initial designs but with the same boundary conditions. Fig. 11 shows the evolution of the design for two other models of different initial fold patterns. In contrast to the example above in Fig. 6, the two designs introduce both the valley and the mountain folds as design variables. In detail, the top group has the same total number of initial folds as Fig. 6, and the bottom group is initially made up of more folding lines. It is worth noting that different initial designs can converge to the same optimum structure with the same imposed boundary conditions. In other words, the proposed method is robust in the sense that it shows little dependency on the initial designs, as shown in Fig. 11.

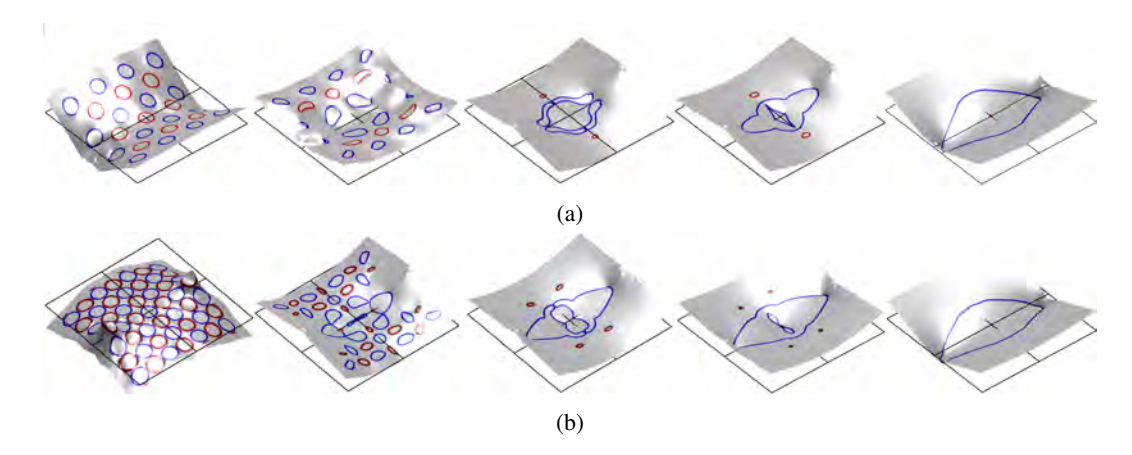


Fig. 11: Left to right: design evolution with different initialization

5.2 The Performance of the Characteristic Objective

As we discussed in Section. 3.2, the characteristic objective is an energy function essential for reaching a design where most deformation happens on the folding lines. In this section, an example is applied to show the effect of the characteristic objective J_2 . The objective function only contains the J_2 with the linear elastic constraint, as shown in the equations:

Minimize:
$$J_2 = \int_{\Omega} \frac{a(\boldsymbol{u}, \, \boldsymbol{u}) - a_{\Gamma}(\boldsymbol{u}, \, \boldsymbol{u})}{a_b(\boldsymbol{u}, \boldsymbol{u})},$$

Subject to: $a(\boldsymbol{u}, \boldsymbol{v}) = l(\boldsymbol{v}), \forall \boldsymbol{v} \in U_{ad}.$ (38)

The design domain is a unit square. Fig. 12 shows the applied boundary conditions (a), the initial design (b) and the achieved result (c). The center of the square is fixed, and two prescribed displacements δ_d in the x-direction are assigned on the two sides to push the model move towards the center; the displacements in other directions are set as zero. The initial design consists of mountain and valley circular folding lines. With the effect of the objective, the design converges from circles to rhombuses. Since the perimeter constraints are not applied, the final result is not smooth and contains zigzags.

Fig.13 is presented to evaluate the performance of the given example. Fig.13.a shows the convergence plot of each parts of the objective function. The solid line plots the total strain energy on the facet area, and the hidden line plots the one over total bending energy in each iteration number. The two plots decrease in the first 20 iterations, then reach convergence and vibrate within a range. Fig. 13.b is the distribution of the strain energy per unit area on the final design. We can observe that the highest number of energy concentrates on the folding lines, which means the deformation mainly occurs on the folding lines.

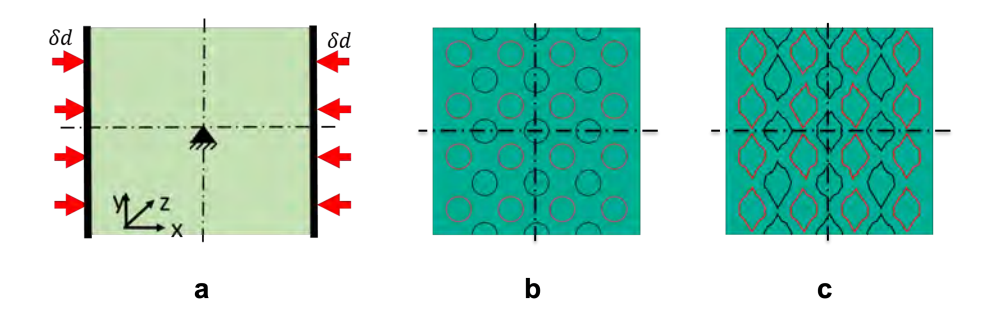


Fig. 12: a. boundary conditions; b. the initial design; c.the final design

6 Conclusions

The purpose of this work is to provide a systematic way of modeling and optimizing an origami-like structure to meet engineering requirements, for instance, transforming force or displacement from one port to another. The origami is physically modeled by a shell model; thus, the in-plane stretching, out-of-plane bending, and shear deformation can be well

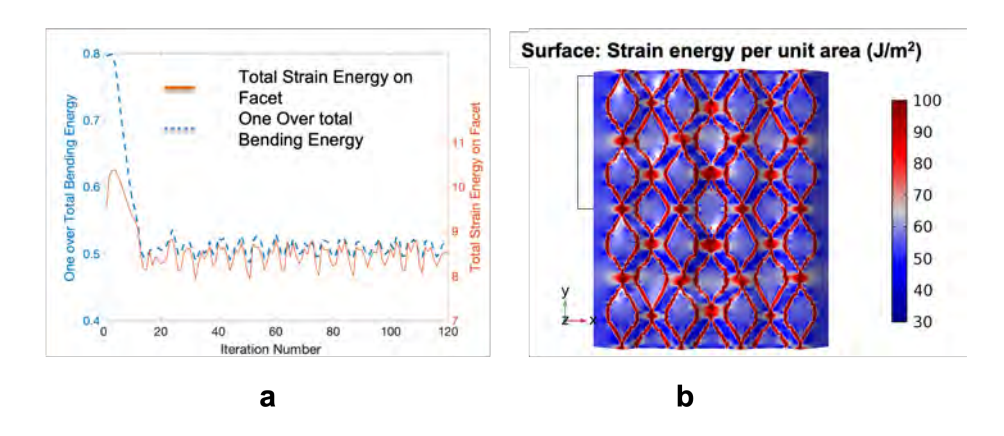


Fig. 13: Left to Right: a. convergence plots; b. unit area strain energy distribution on the final design

captured. Moreover, the folding lines are represented implicitly by the zero contours of the level set functions. Instead of assuming straight folding lines, our model can form curved folding lines, and the straightness of creases can be controlled by the perimeter constraint. An origami gripper, as well as a twisting mechanism, are optimized as demonstrations. The proposed method shows little dependence on the initial crease patterns as long as the boundary conditions are the same.

However, some aspects need to be improved. First, in the current set-up of the problem, the design is based on linear elasticity and small deformation. In the future, we will examine the relatively large non-linear deformation to capture the origami transformation with greater precision. Second, the current formulation of the problem relies mainly on maximizing or minimizing specific energies on the structure. We do not explicitly control the overlapping between mountain and valley folds. The evolution of the design is driven by the velocity field derived from the physics equation. However, one particular type of overlap, or termed vertex, should be discussed. Mathematicians [6] have shown that the number of vertices, mountain, and valley folding lines determines an origami's foldability. The geometrical concerns, such as foldability requirements, need to be coupled into the problem formulation in future work. In addition, the origami structure is optimized as a mechanism triggered by input loads in this work. The behaviors such as self-locking, face overlapping, and folding sequences have to be taken into account.

In terms of applications, the work can be expanded into the design of programmable folding surfaces by considering the manufacture of origami with active materials, such as ferromagnetic particles [58], thermal active polymers, and dielectric elastomers. Under a specific stimulus, it automatically switches between the original state and a target form. Moreover, with the topology optimization framework of free-form surface-the extended level set method [58,59,60,61,62,63], we can optimize conformal origami structures on the surface with desired properties and kinematic performance.

Acknowledgements

This project is supported by the National Science Foundation (CMMI-1762287), the Ford University Research Program (URP) (Award No. 2017-9198R), and the start-up fund from the State University of New York at Stony Brook.

Appendix A

A The Strain Energy Density of a Linear Elastic Shell Structure

In this section, the background information of the linear elastic shell structure is introduced, and the derivation of the strain energy density is presented. Typically, a shell structure consists of a curved external surface as well as a uniform thickness, as shown in Fig. 14. Let ξ_1, ξ_2 be the two curvilinear coordinates in the middle surface, and ξ_3 be the coordinate in the thickness direction varying within [-1 1] [50,51]. Thus, any point on the shell structure can be represented as $\mathbf{x}(\xi_1, \xi_2, \xi_3)$ [64,65].

$$x(\xi_1, \xi_2, \xi_3) = x^n(\xi_1, \xi_2) + \xi_3 \frac{t(\xi_1, \xi_2)}{2} n(\xi_1, \xi_2).$$
(39)

The Jacobian matrix of the mapping between the middle surface and reference surface shown in the left corner at Fig .14, where

$$J = \frac{\partial x_i}{\partial \xi_j}. (40)$$

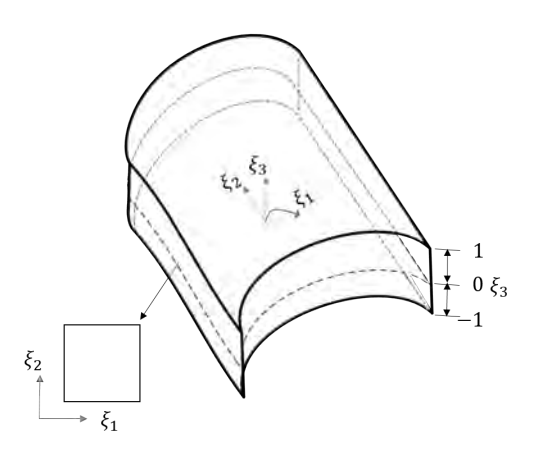


Fig. 14: The schematic figure of shell structure

For linear elastic material, the strain tensor is defined as

$$\varepsilon_{ij}(\mathbf{u}) = \frac{1}{2} \left(\frac{\partial u_i}{\partial x_j} + \frac{\partial u_j}{\partial x_i} \right),
\varepsilon_{ij}(\mathbf{u}) = \frac{1}{2} \left(\frac{\partial u_i}{\partial \xi_m} \frac{\partial \xi_m}{\partial x_j} + \frac{\partial u_j}{\partial \xi_m} \frac{\partial \xi_m}{\partial x_i} \right),$$
(41)

$$\varepsilon_{ij}(\boldsymbol{u}) = \frac{1}{2} \left(\frac{\partial u_i}{\partial \xi_m} \frac{1}{J_{mj}} + \frac{\partial u_j}{\partial \xi_m} \frac{1}{J_{mi}} \right)
= sym \left(\frac{\partial u_i}{\partial \xi_m} J_{mj}^{-1} \right),$$
(42)

where ξ_m represents the reference coordinates. The energy bilinear form for linear elasticity is shown as

$$a(\boldsymbol{u},\boldsymbol{v}) = \int_{\Omega} \varepsilon_{ij}(\boldsymbol{u}) \mathbb{C}_{ijkl} \varepsilon_{kl}(\boldsymbol{v}) d\Omega, \tag{43}$$

where u stands for the displacement, and v is the test function.

According to the Reissner-Mindlin theory of plate [66], we can assume that the displacement along the thickness is linear and the cross section of the shell structure remains flat after deformation. Then the deformation on shell can be written as [67]

$$\mathbf{u} = u^{1}(\xi_{1}, \xi_{2}) + \xi_{3}u^{2}(\xi_{1}, \xi_{2}), \tag{44}$$

where on the right-hand side, the first term represents the membrane deformation, and the second term stands for the bending and shear deformation.

For the thin shell which the thickness is very small and can be neglected, the Jacobian are considered to be a function of only ξ_1, ξ_2 coordinates. Thus the equation (42) can be simplified as [67]:

$$\varepsilon_{ij}(\boldsymbol{u}) = \varepsilon_{ij}^{1}(\boldsymbol{u}) + \xi_{3}\varepsilon_{ij}^{2}(\boldsymbol{u}), \tag{45}$$

where $\varepsilon_{ij}^1(\boldsymbol{u})$ and $\varepsilon_{ij}^2(\boldsymbol{u})$ are the membrane-shear stain and bending strain respectively.

Substitute equation (45) into equation (43) and integrate from $\xi_3 \in [-1,1]$, we can rewrite the energy bilinear form as [56,67]

$$a(\boldsymbol{u},\boldsymbol{v}) = \int_{-1}^{1} \int \int \left[\boldsymbol{\varepsilon}_{ij}^{1}(\boldsymbol{u}) + \boldsymbol{\xi}_{3}\boldsymbol{\varepsilon}_{ij}^{2}(\boldsymbol{u}) \right] \mathbb{C}_{ijkl} \left[\boldsymbol{\varepsilon}_{ij}^{1}(\boldsymbol{v}) + \boldsymbol{\xi}_{3}\boldsymbol{\varepsilon}_{ij}^{2}(\boldsymbol{v}) \right] |\mathbf{J}| d\boldsymbol{\xi}_{1} d\boldsymbol{\xi}_{2} d\boldsymbol{\xi}_{3}$$

$$= \int_{-1}^{1} \int \int \left[\boldsymbol{\varepsilon}_{ij}^{1}(\boldsymbol{u}) \mathbb{C}_{ijkl} \boldsymbol{\varepsilon}_{ij}^{1}(\boldsymbol{v}) + \boldsymbol{\xi}_{3}\boldsymbol{\varepsilon}_{ij}^{1}(\boldsymbol{u}) \mathbb{C}_{ijkl} \boldsymbol{\varepsilon}_{ij}^{2}(\boldsymbol{v}) \right] + \boldsymbol{\xi}_{3}\boldsymbol{\varepsilon}_{ij}^{2}(\boldsymbol{u}) \mathbb{C}_{ijkl} \boldsymbol{\varepsilon}_{ij}^{2}(\boldsymbol{v}) \right] |\mathbf{J}| d\boldsymbol{\xi}_{1} d\boldsymbol{\xi}_{2} d\boldsymbol{\xi}_{3}.$$

$$(46)$$

since the second and third terms are odd functions over the interval $\xi_3 \in [-1, 1]$, and thus equation (46) can be simplified as below [56]

$$a(\boldsymbol{u},\boldsymbol{v}) = \int_{A} [2\varepsilon_{ij}^{1}(\boldsymbol{u})\mathbb{C}_{ijkl}\varepsilon_{kl}^{1}(\boldsymbol{v})|\mathbf{J}| + \frac{2}{3}\varepsilon_{ij}^{2}(\boldsymbol{u})\mathbb{C}_{ijkl}\varepsilon_{kl}^{2}(\boldsymbol{v})|\mathbf{J}|]dA. \tag{47}$$

where the first term represent the coupled membrane-shear strain energy and the second term donates the bending strain energy. In the later contents, we will use the $a_b(\mathbf{u}, \mathbf{u})$ to represent the bending strain energy.

References

- [1] Turner, N., Goodwine, B., and Sen, M., 2016. "A review of origami applications in mechanical engineering". *Proceedings of the Institution of Mechanical Engineers, Part C: Journal of Mechanical Engineering Science*, **230**(14), pp. 2345–2362.
- [2] Overvelde, J. T., De Jong, T. A., Shevchenko, Y., Becerra, S. A., Whitesides, G. M., Weaver, J. C., Hoberman, C., and Bertoldi, K., 2016. "A three-dimensional actuated origami-inspired transformable metamaterial with multiple degrees of freedom". *Nature communications*, 7(1), pp. 1–8.
- [3] Fuchi, K., Diaz, A. R., Rothwell, E. J., Ouedraogo, R. O., and Tang, J., 2012. "An origami tunable metamaterial". *Journal of Applied Physics*, **111**(8), p. 084905.
- [4] Kamrava, S., Mousanezhad, D., Ebrahimi, H., Ghosh, R., and Vaziri, A., 2017. "Origami-based cellular metamaterial with auxetic, bistable, and self-locking properties". *Scientific reports*, 7(1), pp. 1–9.
- [5] Morgan, J., Magleby, S. P., and Howell, L. L., 2016. "An approach to designing origami-adapted aerospace mechanisms". *Journal of Mechanical Design*, **138**(5).
- [6] Ishida, S., Nojima, T., and Hagiwara, I., 2014. "Mathematical approach to model foldable conical structures using conformal mapping". *Journal of mechanical design*, **136**(9).
- [7] Hull, T., 1994. "On the mathematics of flat origamis". Congressus numerantium, pp. 215–224.
- [8] Hull, T. C., et al., 2002. "Modelling the folding of paper into three dimensions using affine transformations". *Linear Algebra and its applications*, **348**(1-3), pp. 273–282.
- [9] Lang, R. J., 1996. "A computational algorithm for origami design". In Proceedings of the twelfth annual symposium on Computational geometry, ACM, pp. 98–105.
- [10] Tachi, T., 2010. "Geometric considerations for the design of rigid origami structures". In Proceedings of the International Association for Shell and Spatial Structures (IASS) Symposium, Vol. 12, Shanghai, pp. 458–460.
- [11] Schenk, M., and Guest, S. D., 2011. "Origami folding: A structural engineering approach". In Origami 5: Fifth International Meeting of Origami Science, Mathematics, and Education, CRC Press, Boca Raton, FL, pp. 291–304.
- [12] Tachi, T., 2009. "Simulation of rigid origami". Origami, 4, pp. 175–187.
- [13] Wei, Z. Y., Guo, Z. V., Dudte, L., Liang, H. Y., and Mahadevan, L., 2013. "Geometric mechanics of periodic pleated origami". *Physical review letters*, **110**(21), p. 215501.
- [14] Lang, R. J., Tolman, K. A., Crampton, E. B., Magleby, S. P., and Howell, L. L., 2018. "A review of thickness-accommodation techniques in origami-inspired engineering". *Applied Mechanics Reviews*, **70**(1).
- [15] Peraza Hernandez, E. A., Hartl, D. J., and Lagoudas, D. C., 2016. "Kinematics of origami structures with smooth folds". *Journal of Mechanisms and Robotics*, **8**(6), p. 061019.
- [16] Hernandez, E. A. P., Hartl, D. J., and Lagoudas, D. C., 2019. "Kinematics of origami structures with smooth folds". In *Active Origami*. Springer, pp. 201–268.
- [17] Liu, K., and Paulino, G. H., 2016. "Merlin: A matlab implementation to capture highly nonlinear behavior of non-rigid origami". In Proceedings of IASS Annual Symposia, Vol. 2016, International Association for Shell and Spatial Structures (IASS), pp. 1–10.
- [18] Liu, K., and Paulino, G., 2017. "Nonlinear mechanics of non-rigid origami: an efficient computational approach". *Proceedings of the Royal Society A: Mathematical, Physical and Engineering Sciences*, **473**(2206), p. 20170348.

- [19] Filipov, E., Liu, K., Tachi, T., Schenk, M., and Paulino, G., 2017. "Bar and hinge models for scalable analysis of origami". *International Journal of Solids and Structures*, **124**, pp. 26–45.
- [20] Ghassaei, A., Demaine, E. D., and Gershenfeld, N., 2018. "Fast, interactive origami simulation using gpu computation". In 7th International Meeting on Origami in Science, Mathematics and Education.
- [21] Gilewski, W., Pełczyński, J., and Stawarz, P., 2014. "A comparative study of origami inspired folded plates". *Procedia Engineering*, **91**, pp. 220–225.
- [22] Cai, J., Ren, Z., Ding, Y., Deng, X., Xu, Y., and Feng, J., 2017. "Deployment simulation of foldable origami membrane structures". *Aerospace Science and Technology*, **67**, pp. 343–353.
- [23] Dias, M. A., Dudte, L. H., Mahadevan, L., and Santangelo, C. D., 2012. "Geometric mechanics of curved crease origami". *Physical review letters*, **109**(11), p. 114301.
- [24] Kilian, M., Flöry, S., Chen, Z., Mitra, N. J., Sheffer, A., and Pottmann, H., 2008. "Curved folding". In ACM transactions on graphics (TOG), Vol. 27, ACM, p. 75.
- [25] Kilian, M., Monszpart, A., and Mitra, N. J., 2017. "String actuated curved folded surfaces". *ACM Transactions on Graphics (TOG)*, **36**(3), p. 25.
- [26] Vergauwen, A., De Laet, L., and De Temmerman, N., 2017. "Computational modelling methods for pliable structures based on curved-line folding". *Computer-Aided Design*, **83**, pp. 51–63.
- [27] Callens, S. J., and Zadpoor, A. A., 2018. "From flat sheets to curved geometries: Origami and kirigami approaches". *Materials Today*, **21**(3), pp. 241–264.
- [28] Bende, N. P., Evans, A. A., Innes-Gold, S., Marin, L. A., Cohen, I., Hayward, R. C., and Santangelo, C. D., 2015. "Geometrically controlled snapping transitions in shells with curved creases". *Proceedings of the National Academy of Sciences*, **112**(36), pp. 11175–11180.
- [29] Nelson, T. G., Lang, R. J., Magleby, S. P., and Howell, L. L., 2016. "Curved-folding-inspired deployable compliant rolling-contact element (d-core)". *Mechanism and Machine Theory*, **96**, pp. 225–238.
- [30] Badger, J. C., Nelson, T. G., Lang, R. J., Halverson, D. M., and Howell, L. L., 2019. "Normalized coordinate equations and an energy method for predicting natural curved-fold configurations". *Journal of Applied Mechanics*, **86**(7).
- [31] Greenwood, J., Avila, A., Howell, L., and Magleby, S., 2020. "Conceptualizing stable states in origami-based devices using an energy visualization approach". *Journal of Mechanical Design*, **142**(9).
- [32] Avila, A., Greenwood, J., Magleby, S. P., and Howell, L. L., 2019. "Conceptualizing stable states in origami-based devices using an energy visualization approach". In ASME 2019 International Design Engineering Technical Conferences and Computers and Information in Engineering Conference, American Society of Mechanical Engineers Digital Collection.
- [33] Fuchi, K., and Diaz, A. R., 2013. "Origami design by topology optimization". Journal of Mechanical Design, 135(11).
- [34] Fuchi, K., Buskohl, P. R., Bazzan, G., Durstock, M. F., Reich, G. W., Vaia, R. A., and Joo, J. J., 2015. "Origami actuator design and networking through crease topology optimization". *Journal of Mechanical Design*, **137**(9), p. 091401.
- [35] Fuchi, K., Buskohl, P. R., Bazzan, G., Durstock, M. F., Reich, G. W., Vaia, R. A., and Joo, J. J., 2016. "Design optimization challenges of origami-based mechanisms with sequenced folding". *Journal of Mechanisms and Robotics*, 8(5)
- [36] Gillman, A. S., Fuchi, K., and Buskohl, P. R., 2019. "Discovering sequenced origami folding through nonlinear mechanics and topology optimization". *Journal of Mechanical Design*, **141**(4).
- [37] Yu, Y., Hong, T.-C. K., Economou, A., and Paulino, G. H., 2021. "Rethinking origami: A generative specification of origami patterns with shape grammars". *Computer-Aided Design*, **137**, p. 103029.
- [38] Suzuki, K., and Kikuchi, N., 1991. "A homogenization method for shape and topology optimization". *Computer methods in applied mechanics and engineering*, **93**(3), pp. 291–318.
- [39] Allaire, G., and Kohn, R., 1993. "Topology optimization and optimal shape design using homogenization". In *Topology design of structures*. Springer, pp. 207–218.
- [40] Nishiwaki, S., Frecker, M. I., Min, S., and Kikuchi, N., 1998. "Topology optimization of compliant mechanisms using the homogenization method". *International journal for numerical methods in engineering*, **42**(3), pp. 535–559.
- [41] Rozvany, G. I., Zhou, M., and Birker, T., 1992. "Generalized shape optimization without homogenization". *Structural optimization*, **4**(3-4), pp. 250–252.
- [42] Bendsoe, M. P., and Sigmund, O., 2013. *Topology optimization: theory, methods, and applications*. Springer Science & Business Media.
- [43] van Dijk, N. P., Maute, K., Langelaar, M., and Van Keulen, F., 2013. "Level-set methods for structural topology optimization: a review". *Structural and Multidisciplinary Optimization*, **48**(3), pp. 437–472.
- [44] Allaire, G., Jouve, F., and Toader, A.-M., 2004. "Structural optimization using sensitivity analysis and a level-set method". *Journal of computational physics*, **194**(1), pp. 363–393.
- [45] Osher, S. J., and Santosa, F., 2001. "Level set methods for optimization problems involving geometry and constraints: I. frequencies of a two-density inhomogeneous drum". *Journal of Computational Physics*, **171**(1), pp. 272–288.
- [46] Allaire, G., Jouve, F., and Toader, A.-M., 2002. "A level-set method for shape optimization". Comptes Rendus Mathe-

- matique, **334**(12), pp. 1125–1130.
- [47] Wang, M. Y., Wang, X., and Guo, D., 2003. "A level set method for structural topology optimization". *Computer methods in applied mechanics and engineering*, **192**(1-2), pp. 227–246.
- [48] Wang, M. Y., and Wang, S., 2006. "Parametric shape and topology optimization with radial basis functions". In IUTAM symposium on topological design optimization of structures, machines and materials, Springer, pp. 13–22.
- [49] Bandi, P., Detwiler, D., Schmiedeler, J. P., and Tovar, A., 2015. "Design of progressively folding thin-walled tubular components using compliant mechanism synthesis". *Thin-Walled Structures*, **95**, pp. 208–220.
- [50] Zhu, J., 2013. The finite element method: its basis and fundamentals. Elsevier.
- [51] Zienkiewicz, O. C., and Taylor, R. L., 2005. The finite element method for solid and structural mechanics. Elsevier.
- [52] Liu, G.-R., and Quek, S. S., 2013. The finite element method: a practical course. Butterworth-Heinemann.
- [53] Bathe, K.-J., and Chapelle, D., 2003. Finite Element Analysis of Shells-Fundamentals. Springer-Verlag Telos.
- [54] Reddy, J. N., 2003. Mechanics of laminated composite plates and shells: theory and analysis. CRC press.
- [55] Yang, K.-H., 2017. Basic finite element method as applied to injury biomechanics. Academic Press.
- [56] Choi, K. K., and Kim, N.-H., 2006. Structural sensitivity analysis and optimization 1: linear systems. Springer Science & Business Media.
- [57] Osher, S., and Fedkiw, R., 2006. *Level set methods and dynamic implicit surfaces*, Vol. 153. Springer Science & Business Media.
- [58] Tian, J., Li, M., Han, Z., Chen, Y., Gu, X. D., Ge, Q., and Chen, S., 2022. "Conformal topology optimization of multi-material ferromagnetic soft active structures using an extended level set method". *Computer Methods in Applied Mechanics and Engineering*, **389**, p. 114394.
- [59] Ye, Q., Guo, Y., Chen, S., Gu, X. D., and Lei, N. "Topology optimization of conformal structures using extended level set methods and conformal geometry theory". In ASME 2018 International Design Engineering Technical Conferences and Computers and Information in Engineering Conference, American Society of Mechanical Engineers Digital Collection.
- [60] Ye, Q., Guo, Y., Chen, S., Lei, N., and Gu, X. D., 2019. "Topology optimization of conformal structures on manifolds using extended level set methods (x-lsm) and conformal geometry theory". *Computer Methods in Applied Mechanics and Engineering*, **344**, pp. 164–185.
- [61] Ye, Q., Jiang, L., Chen, S., and Gu, X., 2018. "Generative design of multifunctional conformal structures using extended level set methods (x-lsm) and conformal geometry theory". In IUTAM Symposium on When Topology Optimization Meets Additive Manufacturing Theory and Methods.
- [62] Ye, Q., Gu, X. D., and Chen, S., 2020. "Generative design of origami-inspired mechanisms with a variational level set approach". In ASME 2020 International Design Engineering Technical Conferences and Computers and Information in Engineering Conference, American Society of Mechanical Engineers Digital Collection.
- [63] Xu, X., Chen, S., Gu, X. D., and Wang, M. Y., 2021. "Conformal topology optimization of heat conduction problems on manifolds using an extended level set method (x-lsm)". In International Design Engineering Technical Conferences and Computers and Information in Engineering Conference, Vol. 85390, American Society of Mechanical Engineers, p. V03BT03A030.
- [64] Ciarlet, P. G., 2005. "An introduction to differential geometry with applications to elasticity". *Journal of Elasticity*, **78**(1-3), pp. 1–215.
- [65] Chapelle, D., and Bathe, K.-J., 2010. *The finite element analysis of shells-fundamentals*. Springer Science & Business Media.
- [66] Papadopoulos, P., and Taylor, R. L., 1990. "A triangular element based on reissner-mindlin plate theory". *International Journal for Numerical Methods in Engineering*, **30**(5), pp. 1029–1049.
- [67] Kim, N. H., Choi, K. K., Chen, J.-S., and Botkin, M. E., 2002. "Meshfree analysis and design sensitivity analysis for shell structures". *International Journal for Numerical Methods in Engineering*, **53**(9), pp. 2087–2116.